

**A novel remitting leukodystrophy associated with a variant
in FBP2**

Journal:	<i>Brain Communications</i>
Manuscript ID	BRAINCOM-2020-362
Manuscript Type:	Original Article
Date Submitted by the Author:	20-Nov-2020
Complete List of Authors:	Gizak, Agnieszka; University of Wroclaw, Department of Molecular Physiology and Neurobiology Diegmann, Susann; University Medical Center Göttingen, Pediatrics Dreha-Kulaczewski, Steffi; University Medical Center Göttingen, Paediatrics and Paediatric Neurology Wiśniewski, Janusz; University of Wroclaw, Department of Molecular Physiology and Neurobiology Duda, Przemysław; University of Wroclaw, Department of Molecular Physiology and Neurobiology Ohlenbusch, Andreas; University Medical Center Göttingen, Pediatric Neurology Huppke, Brenda; University Medical Center Göttingen, Pediatric Neurology Henneke, Marco; University Medical Center Göttingen, Pediatric Neurology Höhne, Wolfgang; Charité – University Medicine Berlin, Institute of Biochemistry Altmüller, Janine; University of Cologne, Cologne Center for Genomics (CCG) Thiele, Holger; University of Cologne, Cologne Center for Genomics (CCG) Nürnberg, Peter; University of Cologne, Cologne Center for Genomics (CCG) Rakus, Darius; University of Wroclaw, Department of Molecular Physiology and Neurobiology Gaertner, Jutta; University Medical Center Göttingen, Pediatric Neurology Huppke, Peter; University Medical Center Göttingen, Pediatric Neurology
Keywords:	

A novel remitting leukodystrophy associated with a variant in *FBP2*

Short title: A remitting leukodystrophy with a FBP2 variant

Agnieszka Gizak^{1#}, Susann Diegmann^{2#}, Steffi Dreha-Kulaczewski², Janusz Wiśniewski¹, Przemysław Duda¹, Andreas Ohlenbusch², Brenda Huppke², Marco Henneke², Wolfgang Höhne³, Janine Altmüller³, Holger Thiele³, Peter Nürnberg³, Dariusz Rakus^{1*}, Jutta Gärtner^{2*}, Peter Huppke^{2*}

contributed equally

* co-corresponding authors

Affiliations

¹ Department of Molecular Physiology and Neurobiology, University of Wrocław, 50-335 Wrocław, Poland.

² Department of Pediatrics and Pediatric Neurology, University Medical Center Göttingen, Georg August University Göttingen, Germany.

³ Cologne Center for Genomics (CCG) and Center for Molecular Medicine Cologne (CMMC), University of Cologne, Faculty of Medicine and University Hospital Cologne, 50931 Cologne, Germany.

1
2
3 Corresponding authors:
4

5 Peter Huppke
6

7
8 Department of Pediatrics and Adolescent Medicine, Pediatric Neurology, University Medical
9 Center Göttingen, Georg August University, Robert-Koch-Strasse 40, 37075 Göttingen,
10 Germany. Fax: 0049551396252, Phone: 00495513913872
11
12

13
14 Jutta Gärtner
15

16 Department of Pediatrics and Adolescent Medicine, Pediatric Neurology, University Medical
17 Center Göttingen, Georg August University, Robert-Koch-Strasse 40, 37075 Göttingen,
18 Germany. 0049551396252, Phone: 0049551393085
19
20

21
22 Dariusz Rakus
23

24 Department of Molecular Physiology and Neurobiology, University of Wrocław, 50-335
25 Wrocław, Poland. Fax: 0048713222817; Phone: 0048713754053.
26
27
28
29
30
31
32
33
34
35
36
37
38
39
40
41
42
43
44
45
46
47
48
49
50
51
52
53
54
55
56
57
58
59
60

Abstract:

Leukodystrophies are genetic disorders of cerebral white matter that almost exclusively have a progressive disease course. We became aware of three members of a family with a disorder characterized by a sudden loss of all previously acquired abilities around one year of age followed by almost complete recovery within two years. Cerebral MRI and myelin sensitive imaging showed a pronounced demyelination that progressed for several months despite signs of clinical improvement and was followed by remyelination. Exome sequencing did not identify any mutations in known leukodystrophy genes but revealed a heterozygous variant in the *FBP2* gene, c.343G>A, p.Val115Met, shared by the affected family members. Cerebral MRI of other family members demonstrated similar white matter abnormalities in all carriers of the variant in *FBP2*. The *FBP2* gene codes for muscle fructose 1,6-bisphosphatase (FBP2), an enzyme involved in gluconeogenesis that is highly expressed in brain tissue. Biochemical analysis showed that the variant has a dominant negative effect on enzymatic activity, substrate affinity, cooperativity and thermal stability. Moreover, it also affects the non-canonical functions of FBP2 involved in mitochondrial protection and regulation of several nuclear processes. In patients' fibroblasts, FBP2 shows no colocalization with mitochondria and nuclei leading to increased reactive oxygen species (ROS) production and a disturbed mitochondrial network. In conclusion, the results of this study indicate that the variant in *FBP2* disturbs cerebral energy metabolism and is associated with a novel remitting leukodystrophy.

Key words: Leukodystrophy, remitting, muscle fructose 1,6-bisphosphatase

Abbreviations:

ADC	apparent diffusion coefficient
ERAD	endoplasmic reticulum-associated protein degradation
ERLAD	ER-to-lysosomes-associated degradation
F-1,6-BP	fructose-1,6-bisphosphate
FBP1	fructose 1,6-bisphosphatase
FBP2	muscle fructose 1,6-bisphosphatase
HCF	healthy control fibroblasts

MRS	Magnetic Resonance Spectroscopy
MT	magnetization transfer
MTsat	MT saturation
ROS	reactive oxygen species
WM	white matter

Introduction

Leukodystrophies are a group of genetic disorders with primary involvement of the central nervous system white matter (van der Knaap and Bugiani, 2017). Most of these disorders have a progressive neurodegenerative course often leading to premature death. Four leukodystrophies with a remitting course have, however, recently been described: 1) Patients with variants in the *TMEM63A* gene, coding for a mechanosensitive ion channel, present with congenital nystagmus and motor delay in infancy associated with hypomyelination of the CNS (Yan *et al.*, 2019). During infancy the myelin deficit resolves, and the clinical course is favorable. 2) Variants in the *SLC13A3* gene, encoding the plasma membrane Na⁺/dicarboxylate cotransporter 3, have been associated with a reversible leukoencephalopathy during febrile illness (Dewulf *et al.*, 2019). Clinical recovery was observed within days of the crisis and MRI changes normalized. 3) Recessive mutations in *GLIALCAM* cause a classical megalencephalic leukoencephalopathy with subcortical cysts. Autosomal dominant mutations in the same gene, however, have been associated with a remitting phenotype (Lopez-Hernandez *et al.*, 2011). 4) Finally, two families with mutations in *FDX2*, coding for a protein involved in mitochondrial [Fe-S] protein assembly, have recently been described in whom partial resolution of the leukoencephalopathy was reported but the clinical course remained progressive (Gurgel-Giannetti *et al.*, 2018).

In this article, we describe a family with a disorder that can also be classified as a remitting leukodystrophy. Affected family members presented with very pronounced white matter abnormalities that almost completely resolved over time, accompanied by remarkable clinical improvement. A missense variant of the *FBP2* gene coding for the muscle fructose 1,6-bisphosphatase (FBP2) segregates with the disorder. FBP is a regulatory enzyme of gluconeogenesis that catalyzes the hydrolysis of fructose-1,6-bisphosphate (F-1,6-BP) to fructose-6-phosphate (F-6-P) and inorganic phosphate. In contrast to the liver isozyme, fructose

1
2
3 1,6-bisphosphatase (FBP1), which regulates glucose production in the liver, kidney and jejunum,
4 FBP2 expression is not restricted to gluconeogenic tissues but is ubiquitous (Al-Robaiy and
5 Eschrich, 1999). Crystallographic studies have demonstrated that FBP2 is a homotetrameric
6 protein which may exist in two quaternary conformations: an active cross-like structure R-state,
7 and an inactive T-state (Barciszewski *et al.*, 2016). Allosteric inhibitors such as AMP and
8 NAD⁺ stabilize the tetrameric conformation of FBP2 and induce a shift towards the T-state
9 (Barciszewski *et al.*, 2016). The capability of FBP2 to adopt various quaternary conformations
10 determines its potential to interact with different cellular binding partners and assume different
11 cellular roles depending on the metabolic and physiological conditions.
12
13
14
15
16
17
18

19 During the last decade it has been shown that FBP2 has also acquired additional functions as a
20 moonlighting protein. The non-canonical functions include FBP2 association with
21 mitochondrial proteins in GSK3 β - in a calcium-dependent manner, thereby making the protein
22 instrumental in the protection of organelles against stress stimuli (Gizak *et al.*, 2012).
23 Furthermore, FBP2 is known to localize in nuclei where it is involved in the regulation of cell
24 mortality and survival. Biochemical and clinical evidence suggests that the variant of FBP2
25 detected in the family described in this article acts in a dominant negative fashion, affecting
26 both enzymatic activity and the non-canonical functions of the enzyme.
27
28
29
30
31
32
33
34
35

36 **Methods**

37
38
39 DNA samples were obtained following informed consent according to the Declaration of
40 Helsinki and approval by the ethic commission from the University Medical Center Göttingen,
41 Göttingen (approval number 2516). Fibroblasts from affected individuals used in this study
42 were obtained from skin biopsies previously sampled for routine diagnostic testing.
43
44
45
46
47
48

49 **Proton Magnetic Resonance Spectroscopy**

50
51 Our multimodal MR-protocol included single-voxel proton Magnetic Resonance Spectroscopy
52 (MRS). Proton MR spectra (64 accumulations) were acquired with use of a STEAM
53 localization sequence with repetition time/echo time/mixing time = 6000/20/10 ms as described
54 (Frahm *et al.*, 1989). Studies older than 15 years were conducted at 2 T (Magnetom Vision;
55 Siemens Medical Solutions, Erlangen, Germany) all others at 3 T (Magnetom Trio, TIM TRIO
56 and Prisma Fit; Siemens Healthcare). The 4.85 ml (2 T) and 4.1 ml (3 T) volumes-of-interest
57
58
59
60

1
2
3 were placed within the parieto-occipital white matter (left or right) covering structural lesions.
4 Absolute concentrations of lactate were determined by LCModel (Provencher, 1993). Normal
5 ranges were taken from Pouwels et al. and our own data base (Pouwels *et al.*, 1999).
6
7
8
9

10 11 **Magnetization Transfer-Imaging**

12
13 Whole brain magnetization transfer (MT)-imaging, as another part of our myelin specific MR-
14 imaging protocol, was performed at 3 T (Magnetom TIM TRIO and Prisma Fit) using a 3D
15 FLASH sequence with 1.25 mm isotropic resolution and 240 mm field-of-view. MT contrast
16 was imposed upon a proton density -weighted reference (TR/TE/ α = 25/4.9 ms/5°, using partial
17 acquisition techniques) by applying a 12.8 ms Gaussian MT-pulse of 540° nominal flip angle
18 2.2 kHz off resonance prior to excitation. By means of a second T1-weighted reference
19 (TR/ α =11 ms/15°, 1.5 minutes), maps of the percentage MT saturation (MTsat) were
20 calculated, a semi-quantitative MT-parameter as described in Helms et al (Helms *et al.*, 2008b).
21 Data processing was scripted using the routines of the FSL 4.1 software library of the Center
22 for Functional Magnetic Resonance Imaging of the Brain (FMRIB, Oxford, UK,
23 www.fmrib.ox.ac.uk/fsl) (Helms *et al.*, 2008a, 2010). The blue-gray-red-yellow color scale of
24 the MTsat maps covered a range from -0.1 pu (light blue; lower limit of the CSF mode) to 1.2
25 pu (gray, gray matter) to 2.5 pu (yellow; fully myelinated white matter)(Dreha-Kulaczewski *et*
26 *al.*, 2012).
27
28
29
30
31
32
33
34
35
36
37
38
39
40

41 **Sequencing of mitochondrial DNA**

42
43 Genomic DNA was extracted from peripheral blood from patient III.5 using standard
44 techniques. Two overlapping mtDNA fragments of 11 and 9 kb encompassing the entire
45 mitochondrial genome were generated with the Expand Long Template PCR System (Roche,
46 Mannheim, Germany) according to the recommendations of the manufacturer. Sanger
47 sequencing was performed using the BigDye™ Terminator v3.1 Cycle Sequencing chemistry
48 on an Applied Biosystems 3500 Genetic Analyzer platform (Applied Biosystems, Darmstadt,
49 Germany). Analyzed sequences were compared with reference NCBI data, accession number
50 NC_012920.1. Primer sequences as well as PCR and sequencing conditions are available on
51 request.
52
53
54
55
56
57
58
59
60

Whole Exome Sequencing

Whole exome sequencing was performed on DNA from EDTA blood of six affected family members (II.2, II.4, III.2, III.4, III.5, IV.1, Figure 1). Each Sequencing barcoded library was prepared using the Agilent SureSelect V6 enrichment Kit. Purified and quantified library pool was subsequently sequenced on an Illumina HighSeq 4000 sequencing instrument (Illumina, San Diego, CA, USA) using a paired end 2x 75bp to 2x 101bp protocol and an allocation of 6 exomes per lane. Data processing, analysis and filtering were performed using the Varbank 2' GUI and pipeline version 3.4/3.5 (CCG, University of Cologne, Germany). Reads were mapped to the human genome reference build GRCh38 using the BWA-MEM alignment algorithm. GATK HaplotypeCaller, Samtools mpileup and Platypus variation calls were filtered for high-quality (QD>5; ARF>0.25; MQ>50; FS<40; MQRankSum>-5; ReadPosRankSum>-5; passed VQSR filter) rare (MAF \leq 0.005 based on the maximum observed population allele frequency in gnomAD v2) variants, predicted to modify a protein sequence or to impair splicing, implicated by reduced maximum entropy scores (MaxEntScan)(Li *et al.*, 2009; McKenna *et al.*, 2010; Rimmer *et al.*, 2014).

For detection of the common genetic cause of all affected family members the dataset was filtered for rare common genetic variants. False positive and irrelevant variants were further reduced by taking advantage of our InHouseDB. The pathogenicity of all received variants was evaluated using several *in silico* analysis tools by the dbNSFP/dbscSNV version 3.4 database.

Validation of variant of interest in *FBP2* as well as co-segregation analysis within the family was performed using Sanger sequencing.

FBP2 expression, mutagenesis and fluorescent labeling

Human FBP2 mutant V115M was created using the procedure described earlier. The following primer pairs were used: FW: AAG AGG GGG AAA TAC ATG GTC TGC TTT GAC C; RV: GGT CAA AGC AGA CCA TGT ATT TCC CCC TCT T. Sequences were confirmed by DNA sequencing using T7 promoter and T7 terminator primers.

WT-FBP2 and V115M-FBP2 were isolated according to Wisniewski *et al.*⁹. Both FBP2 variants were labeled using FITC as described previously (Wisniewski *et al.*, 2017).

Enzyme activity measurements

FBP2 activity was measured at pH 7.5 and 37°C using a glucose 6-phosphate isomerase—glucose 6-phosphate dehydrogenase coupled assay and the reduction of NADP⁺ to NADPH

1
2
3 was monitored spectrophotometrically at 340 nm (Zarzycki *et al.*, 2011). Parameters were
4 estimated in MATLAB's curve fitting tool, using nonlinear least squares regression with trust-
5 region algorithm and bisquare robust fitting.
6
7

8 FBP2 inhibition by AMP was measured in triplicate for each concentration of the ligand.
9
10

11 **Protein melting assay**

12 Protein precipitation was assessed by measurement of light scattering at 600 nm wavelength
13 using an Agilent 8453 UV-Vis spectrophotometer with 10 mm light path length. The
14 measurements were conducted at temperatures ranging from 35°C to 80°C in 2°C steps.
15 Samples were equilibrated for 2 min before each measurement. To avoid sedimentation, the
16 samples were stirred at 200 rev min⁻¹. Buffer and protein concentration were the same as in the
17 enzymatic activity measurements. 300 μM AMP was added for T-state measurements. To
18 determine the melting temperatures, derivative curves of absorbance versus temperature were
19 calculated. The maxima of the derivative curves correspond to the melting temperatures.
20
21
22
23
24
25
26
27
28

29 **Cell culturing**

30 Fibroblasts were cultured as we described before (Duda *et al.*, 2020).
31
32
33

34 **Fluorescent In Situ Hybridization (FISH)**

35 FISH was performed as described in (Mamczur *et al.*, 2015). The following oligonucleotides
36 complementary to human mRNA sequences were used: WT-FBP2 (5'-(Cyanine3) CCT CAG
37 GGA ATT TCT TTT TCT GCA CAT ATC CAG TGG TGG C-3'), V115M-FBP2 (5'-
38 (Cyanine5) CCA GTG GGT CAA AGC ACA TCA CGT ATT TCC CCC GCT TCT C-3'). All
39 the oligonucleotides were synthesized by Merck KGaA. In controls, the oligonucleotide probes
40 were omitted.
41
42
43
44
45
46
47

48 **Immunocytochemistry**

49 Cells growing on coverslips were fixed in 4% paraformaldehyde, permeabilized with 0.1%
50 Triton X-100 in PBS and incubated with 3% BSA in PBS to reduce nonspecific binding of
51 antibodies. Then they were incubated with the respective primary antibody: mouse monoclonal
52 to PSMC6 (1:500, Abcam, Cambridge, UK, ab22639), mouse monoclonal to LAMP-1 (1:500,
53 Santa Cruz Biotechnology, Dallas, TX, USA, sc-20011), rabbit polyclonal to FBP (1:500,
54 purified and characterized as described in (Gizak and Dzugaj, 2003)).
55
56
57
58
59
60

1
2
3 The primary antibodies were then detected using fluorophore-labeled secondary antibodies:
4 goat polyclonal to mouse IgG (AlexaFluor488) (1:1000; Abcam, Cambridge, UK, ab150113),
5 goat polyclonal to mouse IgG (AlexaFluor633) (1:1000; ThermoFisher Scientific, Waltham,
6 MA, USA, a21050), goat polyclonal to rabbit IgG (AlexaFluor488) (1:1000; ThermoFisher
7 Scientific, Waltham, MA, USA, a11034), goat polyclonal to rabbit IgG (AlexaFluor633)
8 (1:1000; ThermoFisher Scientific, Waltham, MA, USA, a21070). To visualize mitochondria,
9 the cells were counterstained with MitoTracker Deep Red (ThermoFisher). In the controls, the
10 primary antibodies were omitted.

11 Images were acquired using FV-1000 confocal microscope (Olympus) with $\times 60$ (oil, Plan
12 SApo, NA = 1.35) objective using the Sequential scan option. The quantification of
13 fluorescence signal was performed using the ImageJ software (Schneider *et al.*, 2012). The cells
14 were marked and the mean fluorescence within the marked areas was measured. The
15 measurements were taken from at least 50 cells from randomly selected areas. Results are
16 expressed as a mean and standard deviation. If not stated otherwise, data were checked for
17 normality using the Shapiro–Wilk test, for equality of variations using the F-test, and for the
18 evaluation of statistical significance the two-tailed Student’s T-test was used. A probability of
19 $p < 0.05$ was considered to represent a significant difference. All the experiments were done at
20 least in triplicate.

21 **Measurements of cellular ROS production and mitochondrial polarization**

22 Cellular ROS production was measured using dihydrofluorescein diacetate (H2DCF-AC) as
23 described in (Gizak *et al.*, 2020). Briefly, live cells were loaded with 5 μM H2DCF-AC (20
24 min, 37°C), rinsed with Hank’s Balanced Salt Solution, and mounted on slides. The
25 fluorescence of the dye was excited at 488 nm for 500 ms. Mitochondrial ROS production was
26 determined by MitoTracker Red CM-H2XRos (ThermoFisher) that fluoresces only upon
27 oxidation.

28 Loss of the mitochondrial membrane potential was detected using JC-1 fluorescent dye
29 (Mitochondrial Permeability Transition Detection Kit, AbD Serotec) according to the
30 manufacturer’s instruction. Polarized mitochondria accumulate more of the dye and are red. In
31 cells with depolarized mitochondria, most of the dye is dispersed in cytoplasm and has green
32 fluorescence. The ratio of red to green fluorescence reflects the degree of the mitochondrial
33 membrane polarization. The JC-1 dye was excited at 488 nm for 500 ms and the emission was
34 observed using a long pass filter, which allowed for simultaneous observation of green
35 (monomers) and red (aggregates) fluorescence.

Protein delivery to fibroblasts and assessment of ERAD activity

Healthy fibroblasts were grown on coverslips. FITC-labeled FBP2 forms were delivered into the cells using CHARIOT Protein Delivery Reagent (Active Motif) as we described before (Wisniewski *et al.*, 2017). Then the cells were counterstained with MitoTracker Deep Red FM or with ER-Tracker Blue White (ThermoFisher) and examined under confocal microscope; in the images, they are shown in red. To test the endoplasmic reticulum-associated degradation of the V115M-FBP2 mutant, healthy fibroblasts were pre-incubated for 1 h with 8 μ M Eeyarestatin, the inhibitor of ERAD (endoplasmic reticulum-associated protein degradation), and transfected with the mutant form of FBP2 in the presence of the inhibitor.

Co-immunoprecipitation

In the co-immunoprecipitation experiment, the cell lysates obtained from cell cultures were used. Briefly, the lysates (100 μ g protein) were mixed and incubated overnight at 4°C with 50 μ g/mL of antibodies against ubiquitin (Lys48-specific, Merck KGaA, Darmstadt, Germany, 05-1307). The complexes were precipitated using 200 μ L/mL of the Protein G Agarose (Merck). The precipitates were centrifuged at 4000 \times g for 2 min and washed with PBS. In control reactions, the precipitating antibodies were omitted. The precipitates were then resuspended in the Laemmli's buffer, resolved by SDS-PAGE, and Western Blot analyses were performed with the use of primary antibodies detecting FBP (isolated and purified as described in (Gizak and Dzugaj, 2003)).

Results

Case reports:

The four-generation pedigree is shown in Fig. 1. Case reports and description of the MRI findings of the family members who did not present with a crisis at age one year are included in figure legends 1 and 2 respectively.

Case reports of the three patients with a remitting leukoencephalopathy in infancy

Patient III.2, female, was born at term after an uneventful pregnancy. Psychomotor development was normal until age 13 months when, during a bronchitis episode with fever, she developed a paresis of the left leg followed within days by the loss of almost all abilities. At presentation to hospital she was irritable, socially withdrawn, unable to sit, crawl or stand and

1
2
3 displayed only minimal motor activity. Significant feeding difficulties made tube feeding
4 necessary for 4 weeks. On examination muscle tone in the legs was increased, while otherwise
5 decreased. First cerebral MRI was performed at age 14 months and showed a leukodystrophy
6 affecting most of the supratentorial white matter with sparing of the periventricular and
7 infratentorial white matter (Fig. 2A). Over the next 11 months she made a slow but continuous
8 recovery. At age 16 months she was able to fixate and hold objects again but was still unable
9 to sit unsupported. By age 24 months no remaining abnormalities were found on neurological
10 examination. Consistent with the clinical findings, a drastic improvement in white matter
11 abnormalities was seen on cerebral MRI performed at age 23 months. The patient is now 25
12 years old and works as a kindergarten teacher. Her only residual deficit is a very mild gait
13 abnormality. Only residual gliotic lesions affecting the corpus callosum and periventricular
14 white matter were seen on cerebral MRI at age 20 years (Fig. 2C).

15
16 Patient III.5, female, was born after an uneventful pregnancy and developed normally until age
17 10 months when all abilities were rapidly lost during a febrile illness. Like patient III.2, she
18 was very irritable, showed no social contact and refused to eat necessitating tube feeding for
19 four months. Muscle tone in the legs was increased, while otherwise decreased. Cerebral MRI
20 at age 11 months also showed a leukodystrophy with pronounced signal changes affecting the
21 deep cerebral white matter and to a lesser extent the nucleus dentatus (Fig. 2D). Over the
22 following 20 months a slow but continuous improvement in her condition was observed. At age
23 17 months she was able to sit unsupported again and speak single words, at 21 months she could
24 walk short distances and speak 2-word sentences and at 30 months her only reported deficit
25 was an inability to run fast. In contrast to the positive clinical development, MRI imaging
26 initially showed a further progression of white matter abnormalities until age 21 months (Fig.
27 2E) before gradually almost completely resolving. Between age 8 and 10 years four focal
28 seizures were reported. Now at age 24 years she works as a social worker, has a slight gait
29 abnormality and avoids walking long distances. Only residual white matter changes remain on
30 cerebral MRI (Fig. 2G).

31
32 Patient IV.1, female, daughter of patient III.5, was born after an uneventful pregnancy at term.
33 After an initial normal period of development, her ability to sit, crawl and walk with support
34 was lost within two days coinciding with a viral infection at age 12 months. She was very
35 irritable, lying with extended, crossed legs. As in the two previous cases, the acute episode was
36 followed by a gradual recovery of lost abilities. At 18 months she was able to sit unsupported
37 again, crawl slowly and stand with support. When last seen at age 21 months she was walking
38 short distances unsupported but speaking only a few single words. Cerebral MRIs obtained over
39
40
41
42
43
44
45
46
47
48
49
50
51
52
53
54
55
56
57
58
59
60

1
2
3 a follow-up period of 16 months displayed a pattern of white matter abnormalities that resemble
4 those seen in patients III.2 and III.5 (Fig. 2H-K). T2 hyperintensities were most pronounced in
5 the centrum semiovale with a central strand of more normal appearing white matter.
6 Interestingly, the apparent diffusion coefficient (ADC) of the initial MRI study performed
7 shortly after onset of symptoms revealed widespread distinctly restricted diffusion in the T2
8 lesional areas (Fig. 2L). In follow up studies the ADC signal then reversed to bright intensities
9 indicating enhanced diffusion (Fig. 2M-O).

10
11
12
13
14
15
16 None of the patients displayed any dysmorphic features and somatic growth including head
17 circumference was normal. In all three patients an extensive diagnostic work-up was performed.
18 Analysis of plasma lactate in the acute stage was normal in patient III.2 but elevated in patient
19 III.5 (3.8 mmol/l) and patient IV.1 (3.5 mmol/l) (reference 0.5-2.2 mmol/l). Normal values were
20 seen for lactate in CSF (III.2, III.5, IV.1), CSF Protein (III.2, III.5, IV.1), copper, ceruloplasmin
21 (III.2, III.5), carbohydrate-deficient transferrin (III.5, IV.1), carnitine and acylcarnitine (III.5,
22 IV.1), very long chain fatty acids (III.2, III.5, IV.1), enzyme activities of arylsulfatase A, beta-
23 galactosidase, hexosaminidase A, hexosaminidase B, galactosylceramidase (III.2, III.5, IV.1),
24 amino acids in CSF and plasma (III.5, IV.1) and organic acids in urine (III.5).

25
26
27
28
29
30
31
32 Biopsy of skin and muscle from patient III.5 was performed. Activities of pyruvate
33 dehydrogenase complex and respiratory chain enzymes in fibroblasts showed moderately
34 reduced activities of complex III and complex IV in fibroblasts and reduced activities of
35 complex II, III and IV in muscle. Muscle histology showed no abnormalities, in particular no
36 ragged red fibers.

37
38
39
40
41 Nerve conduction velocity (III.2, III.5, IV.1) as well as acoustic evoked potentials (III.2, III.5,
42 IV.1) were repeatedly normal. Visual evoked potentials were normal in III.2 and abnormal in
43 III.5 and IV.1 in the acute phase.
44
45
46
47
48

49 **Proton MR-spectroscopy and Myelin sensitive imaging indicate** 50 **mitochondrial failure and demyelination during the acute phase and** 51 **subsequent recovery** 52 53 54

55
56
57
58
59
60
61
62
63
64
65
66
67
68
69
70
71
72
73
74
75
76
77
78
79
80
81
82
83
84
85
86
87
88
89
90
91
92
93
94
95
96
97
98
99
100
101
102
103
104
105
106
107
108
109
110
111
112
113
114
115
116
117
118
119
120
121
122
123
124
125
126
127
128
129
130
131
132
133
134
135
136
137
138
139
140
141
142
143
144
145
146
147
148
149
150
151
152
153
154
155
156
157
158
159
160
161
162
163
164
165
166
167
168
169
170
171
172
173
174
175
176
177
178
179
180
181
182
183
184
185
186
187
188
189
190
191
192
193
194
195
196
197
198
199
200
201
202
203
204
205
206
207
208
209
210
211
212
213
214
215
216
217
218
219
220
221
222
223
224
225
226
227
228
229
230
231
232
233
234
235
236
237
238
239
240
241
242
243
244
245
246
247
248
249
250
251
252
253
254
255
256
257
258
259
260
261
262
263
264
265
266
267
268
269
270
271
272
273
274
275
276
277
278
279
280
281
282
283
284
285
286
287
288
289
290
291
292
293
294
295
296
297
298
299
300
301
302
303
304
305
306
307
308
309
310
311
312
313
314
315
316
317
318
319
320
321
322
323
324
325
326
327
328
329
330
331
332
333
334
335
336
337
338
339
340
341
342
343
344
345
346
347
348
349
350
351
352
353
354
355
356
357
358
359
360
361
362
363
364
365
366
367
368
369
370
371
372
373
374
375
376
377
378
379
380
381
382
383
384
385
386
387
388
389
390
391
392
393
394
395
396
397
398
399
400
401
402
403
404
405
406
407
408
409
410
411
412
413
414
415
416
417
418
419
420
421
422
423
424
425
426
427
428
429
430
431
432
433
434
435
436
437
438
439
440
441
442
443
444
445
446
447
448
449
450
451
452
453
454
455
456
457
458
459
460
461
462
463
464
465
466
467
468
469
470
471
472
473
474
475
476
477
478
479
480
481
482
483
484
485
486
487
488
489
490
491
492
493
494
495
496
497
498
499
500
501
502
503
504
505
506
507
508
509
510
511
512
513
514
515
516
517
518
519
520
521
522
523
524
525
526
527
528
529
530
531
532
533
534
535
536
537
538
539
540
541
542
543
544
545
546
547
548
549
550
551
552
553
554
555
556
557
558
559
560
561
562
563
564
565
566
567
568
569
570
571
572
573
574
575
576
577
578
579
580
581
582
583
584
585
586
587
588
589
590
591
592
593
594
595
596
597
598
599
600
601
602
603
604
605
606
607
608
609
610
611
612
613
614
615
616
617
618
619
620
621
622
623
624
625
626
627
628
629
630
631
632
633
634
635
636
637
638
639
640
641
642
643
644
645
646
647
648
649
650
651
652
653
654
655
656
657
658
659
660
661
662
663
664
665
666
667
668
669
670
671
672
673
674
675
676
677
678
679
680
681
682
683
684
685
686
687
688
689
690
691
692
693
694
695
696
697
698
699
700
701
702
703
704
705
706
707
708
709
710
711
712
713
714
715
716
717
718
719
720
721
722
723
724
725
726
727
728
729
730
731
732
733
734
735
736
737
738
739
740
741
742
743
744
745
746
747
748
749
750
751
752
753
754
755
756
757
758
759
760
761
762
763
764
765
766
767
768
769
770
771
772
773
774
775
776
777
778
779
780
781
782
783
784
785
786
787
788
789
790
791
792
793
794
795
796
797
798
799
800
801
802
803
804
805
806
807
808
809
810
811
812
813
814
815
816
817
818
819
820
821
822
823
824
825
826
827
828
829
830
831
832
833
834
835
836
837
838
839
840
841
842
843
844
845
846
847
848
849
850
851
852
853
854
855
856
857
858
859
860
861
862
863
864
865
866
867
868
869
870
871
872
873
874
875
876
877
878
879
880
881
882
883
884
885
886
887
888
889
890
891
892
893
894
895
896
897
898
899
900
901
902
903
904
905
906
907
908
909
910
911
912
913
914
915
916
917
918
919
920
921
922
923
924
925
926
927
928
929
930
931
932
933
934
935
936
937
938
939
940
941
942
943
944
945
946
947
948
949
950
951
952
953
954
955
956
957
958
959
960
961
962
963
964
965
966
967
968
969
970
971
972
973
974
975
976
977
978
979
980
981
982
983
984
985
986
987
988
989
990
991
992
993
994
995
996
997
998
999
1000

Localized MRS performed in Patients III.2, III.5 and IV.1 shortly after onset of symptoms uniformly revealed lactate elevation in white matter lesions in all three patients. In patient III.5 and her daughter, patient IV.1 follow up MRS were obtained over a period of 14 and 1.3 years

1
2
3 respectively. Results demonstrated a gradual normalization coinciding with the clinical
4 improvement (Fig. 3A).
5
6

7 MTsat maps obtained in IV.1 depicted initial myelin deficit most pronounced in the lesions
8 (blue color-coded white matter (WM) areas, Fig. 3B-D). In comparison to the maps of a younger
9 healthy control (age 1.5 years) in Fig. 3 E the myelin loss appeared more widespread than
10 depicted by conventional T2 weighted imaging (Fig. 2H-K). Subsequent studies six months and
11 1.3 years later indicated progressive demyelination (Fig 3C) followed by remyelination
12 (appearance of gray-red-orange-yellow color-coded WM, Fig 3D)
13
14
15
16
17
18
19
20

21 **Exome sequencing detects a variant in *FBP2* with unknown pathogenicity**

22
23 Because segregation within the family was compatible with maternal inheritance, the complete
24 mitochondrial genome from patient III.5 was sequenced. No variants with known or suspected
25 pathogenicity were detected. Furthermore, no deletions or duplications of mitochondrial DNA
26 were seen.
27
28
29

30
31 Exome sequencing was initially performed in DNA samples from family members, III.2, III.5
32 and IV.1 and later extended to II.2, II.4, III.4 (Supp. Tab. 1). No mutations in known
33 leukodystrophy genes were detected but the analysis revealed heterozygous missense variants
34 common in all patients in *CCT6A* (c.446T>C, p.Ile149Thr) and *FBP2* (c.343G>A,
35 p.Val115Met) (Supp. Tab. 2). The variant in *CCT6A* is a frequent multiallelic site in gnomAD
36 and is predicted to have a benign impact (Supp. Tab. 2). Therefore, it was not considered
37 pathogenic. The variant p.Val115Met in *FBP2* is not described in our in-house population
38 database and only once in a European male in gnomAD (accessed in May 2020) (Allele
39 frequency: 0.000003979). The *FBP2* variant p.Val115Met is predicted to be possibly damaging
40 by 10 out of 13 *in silico* analysis tools (Supp. Tab. 3). Furthermore, the position Val115 is
41 highly conserved both in vertebrate *FBP2* and *FBP1*, and also in *FBPs* of insects and plants, as
42 can be derived from a multiple sequence alignment and is highly conserved in terrestrial
43 vertebrates (Supp. Fig. 2A). Val115 is situated in a hydrophobic pocket formed by the residues
44 Val94, Tyr140, Ala153. Active site and metal binding sites are not directly involved but an
45 exchange of the small valine side chain by the much larger methionine may disturb the structure
46 locally (Suppl. Fig. 2B). Sanger sequencing was performed in all family members who agreed
47 to the analysis (Suppl. Fig. 1A). The *FBP2* variant was confirmed in the family members who
48 had undergone exome sequencing and was also confirmed in patient IV.2 who has subsequently
49
50
51
52
53
54
55
56
57
58
59
60

1
2
3 been shown to have leukoencephalopathy, developmental delay and behavioral problems. It
4 was also detected in patient III.3 who has a history of psychiatric problem but declined MR
5 imaging (Suppl. Fig. 2). The *FBP2* variant was not detected in the only healthy offspring, III.1.
6
7 As the genetic results suggest a causative role of the *FBP2* c.343G>A, p.Val115Met variant in
8
9 the disorder seen in the family we conducted biochemical analyses to support its pathogenicity.
10
11
12
13
14

15 **The V115M-FBP2 variant affects activity, substrate affinity and thermal** 16 **stability of FBP2** 17 18

19
20 The residue 115 is not directly involved in the mechanism of catalysis and allosteric inhibition
21 of FBP2. However, the analysis of kinetic properties of the recombinant protein demonstrated
22 that V115M-FBP2 was about two-fold less active than WT-FBP2 (Fig. 4A), and its affinity to
23 the substrate, F-1,6-BP, was over 1.5 times lower. V115M-FBP2 was also significantly less
24 sensitive to the action of the allosteric inhibitor AMP and the cooperativity of the inhibition
25 was lost. Since the cooperativity of the allosteric inhibition of FBP2 is linked to the mechanism
26 of R-to-T transition and tetramerization, the V115M mutation most likely disrupts the
27 quaternary structure of the protein. Comparison of melting points of V115M-FBP2 and WT-
28 FBP2 using the thermal denaturation method showed that, as in the case of WT-FBP2, the
29 presence of AMP during incubation improved the thermal stability of V115M-FBP2 (Fig. 4B).
30 However, both the AMP-saturated and the AMP-free V115M-FBP2 was significantly less
31 stable than WT-FBP2. To verify these differences, we monitored activities of both enzyme
32 variants during incubation at 37°C. Their activities decreased about two-fold after the first 20-
33 25 hours of incubation, however, during the subsequent 25 hours, activity of WT-FBP2
34 remained unchanged while activity of V115M-FBP2 was constantly decreasing (Fig. 4C).
35
36
37
38
39
40
41
42
43
44
45
46
47
48

49 **The V115M-FBP2 variant alters subcellular localization of FBP2** 50

51 Next, we analyzed the subcellular localization of FBP2 in healthy fibroblasts, and fibroblasts
52 derived from patient III.5. As expected, in healthy control fibroblasts (HCF), FBP2 was
53 localized in cytoplasm where it was relatively homogeneously dispersed in the whole cell. A
54 slightly fibrillar localization of the enzyme might be attributed to co-localization of a fraction
55 of the protein with mitochondria (Gizak *et al.*, 2012). The enzyme was also present in nuclei
56 (Fig. 5A). In contrast, in fibroblasts derived from patient III.5, FBP2 showed granular
57
58
59
60

1
2
3 localization. It was present only within the cells' bodies, not in protrusions, and did not localize
4 in cells' nuclei.
5
6
7
8
9

10 **The V115M-FBP2 variant does not colocalize with mitochondria, correlating** 11 **with disturbance of their network and increase in ROS production** 12 13

14 The localization of FBP2 in cytoplasm seen in fibroblasts from patient III.5, suggested
15 mitochondrial accumulation of the enzyme, but immunostaining revealed that in fact, it did not
16 co-localize with mitochondria, even if the cells were treated with GSK3 β inhibitor (Fig. 5B) or
17 elevated Ca²⁺ concentrations (data not shown) which have been shown to stimulate
18 accumulation of FBP2 on mitochondria (Gizak *et al.*, 2012). Both factors increased
19 colocalization of the FBP2-related fluorescence with mitochondria in HCF. To conclusively
20 demonstrate that the lack of FBP2 colocalization with mitochondria is a result of inability of
21 V115M-FBP2 to interact with the organelles we transfected HCF with FITC-labeled V115M-
22 FBP2 and found no accumulation of the FITC-related fluorescence on mitochondria (Fig. 5C).
23
24
25
26
27
28
29

30 Next, we studied the mitochondrial network in fibroblasts from patient III.5. We found that the
31 network was less developed and mitochondrial membranes were less polarized compared to
32 HCF (Fig. 5D). Moreover, the disturbances in the mitochondrial network were accompanied by
33 an increased production of ROS, both in cytoplasm and in mitochondria.
34
35
36
37
38
39
40

41 **The V115M-FBP2 variant is degraded by ERAD and ER-to-lysosomes-** 42 **associated degradation (ERLAD) pathways** 43 44

45 Surprisingly, the total fluorescent signal associated with polyclonal antibodies against FBP2
46 was much stronger in fibroblasts from patient III.5 than in HCF (Fig. 6A). This raised the
47 question, if the elevation of FBP2-related signal was a result of increased expression of V115M-
48 FBP2 and/or WT-FBP2. Since antibodies against FBP2 do not discriminate between these two
49 variants we used fluorescently labeled oligonucleotides against both forms of FBP2 to quantify
50 their expression. As expected, expression of V115M-FBP was only seen in fibroblasts from
51 patient III.5, but not in HCF, demonstrating specificity of the oligonucleotides (Fig. 6B).
52 Moreover, in fibroblasts from patient III.5, the expression of WT-FBP2 was increased. This
53 prompted us to analyze the colocalization of WT-FBP2 and V115M, with various systems of
54 protein turnover in a cell. We found that transfection of wild type fibroblasts with FITC-labeled
55
56
57
58
59
60

1
2
3 V115M-FBP2 and WT-FBP2 led to colocalization of the mutant protein, but not the WT-FBP2,
4 with the endoplasmic reticulum (ER) (Fig. 6C) ER is a part of the cellular machinery of
5 misfolded protein degradation. Endoplasmic-reticulum-associated protein degradation (ERAD)
6 is a process in which proteins are dislocated from ER to the cytosol for ubiquitylation and
7 proteasomal degradation. Treatment of fibroblasts with the ERAD inhibitor Eeyrestatin
8 decreased the level of FITC-labeled V115M-FBP2 colocalization with ER (Fig. 6C). In line
9 with this, we observed a higher level of FBP2 (the sum WT-FBP2 and V115M-FBP2)
10 polyubiquitylation in fibroblasts from patient III.5 compared to HCF (Fig. 6D). We also found
11 that most of the V115M-FBP2-fluorescence colocalized with PSMC6 protein which is a
12 component of the 26S proteasome, although the total level of PSMC6 in these cells was not
13 elevated (Fig. 6E). It is known that some defective proteins do not engage ERAD machinery
14 because their aggregates are too large and/or cannot be relocated across the ER membrane
15 (ERAD-resistant misfolded proteins)(Houck *et al.*, 2014). The low thermal stability of the
16 V115M-FBP2 and the presence of the enzyme in granule-like structures, suggested that the
17 protein may be only partially eliminated by ERAD. Instead, it may be predominantly cleared
18 by the alternative, ERAD-independent process of misfolded proteins degradation referred to as
19 ELRAD (ER-to-lysosome-associated degradation), involving ER-phagy, microautophagy or
20 vesicular transport (Fregno *et al.*, 2018). One of the indicators of the ELRAD process intensity
21 is the abundance of lysosome-associated membrane glycoprotein 1 (LAMP-1) which represents
22 the major constituent of lysosomal membrane proteins in a cell (Fregno *et al.*, 2018). Results
23 of our study showed that the expression of LAMP-1 protein was over 2.5-times higher in patient
24 III.5 fibroblasts than in HCF (Fig. 6F). This points to ELRAD as the main system involved in
25 the clearance of defective variant of FBP2.
26
27
28
29
30
31
32
33
34
35
36
37
38
39
40
41
42
43
44
45

46 Discussion

47
48 In this article, we describe a family with a novel white matter disease. The three index patients
49 experienced a severe crisis during a febrile illness at age 10-13 months resulting in a loss of all
50 learned abilities. The acute episode was followed by a gradual recovery phase and achievement
51 of normal developmental status within 1-2 years. Little is known about the early childhood of
52 patients II.1 and II.2, as both grew up in an orphanage because their mother was unable to care
53 for them due to a psychiatric disorder. However, of note is that they both display a similar
54 residual MRI pattern to their daughters. A further family member, patient III.4, also has
55 documented reversible white matter changes on repeated MRI imaging. Remarkably, none of
56
57
58
59
60

1
2
3 the index patients has experienced a second attack indicating that there might be a phase of
4 vulnerability in brain development around the end of the first year of life.
5

6
7 Cerebral MRI at the time of the crisis revealed dramatic leukodystrophy of the periventricular
8 white matter and the corpus callosum, more severe than in any of the known remitting
9 leukodystrophies. White matter changes in the T2 weighted images were seen to increase for
10 several months despite clinical improvement. In patient IV.1 DWI, myelin imaging and MRS
11 were performed. DWI in the initial acute phase showed restricted diffusion in the affected white
12 matter indicating cytotoxic edema consistent with a metabolic crisis. This finding was
13 supported by MRS evidence of increased lactate in the white matter. During the following
14 months diffusion was temporarily increased compatible with a reduction of myelin and
15 subsequent remyelination. Consistently, myelin imaging initially demonstrated a massive
16 decrease followed by a gradual increase and almost normalization of white matter myelin. The
17 imaging data together with the clinical course are best compatible with an event associated with
18 massive demyelination followed by remyelination over a period of 1-2 years. The near complete
19 recovery makes preferential neuronal damage unlikely. We therefore hypothesize that the
20 primary affected cells in this disorder are the oligodendrocytes.
21
22

23
24 Following exclusion of mutations in the mitochondrial DNA and in known leukodystrophy
25 genes, exome sequencing resulted in the detection of only one variant that segregated with the
26 leukodystrophy in the family and not frequently reported in current databases; *FBP2* c.343G>A,
27 p.Val115Met. The affected amino acid Val115 is highly conserved in terrestrial vertebrates and
28 is predicted to be damaging. In all available family members, the variant segregated with
29 leukoencephalopathy on Sanger sequencing of the *FBP2* gene. Subject III.1 is the only
30 offspring who carries the WT allele. She has no known neurological disorder and normal cranial
31 MR imaging (data not shown).
32
33

34
35 So far, no human disorders have been linked to variants in the *FBP2* gene. Mutations in *FBP1*,
36 coding for FBP1, a key enzyme of gluconeogenesis that is expressed in liver and kidney, cause
37 fructose-1,6-bisphosphate deficiency, a disorder characterized by recurrent severe metabolic
38 crises after fructose ingestion or during febrile illness. To assess the pathogenicity of the
39 V115M-*FBP2* variant, we investigated enzymatic function, in particular the kinetic properties
40 and stability of the variant. We found that V115M-*FBP2* has reduced activity, thermal stability
41 and substrate affinity. Moreover, the enzyme was less sensitive to the action of allosteric
42 inhibitor AMP and the cooperativity of the inhibition was lost. Under physiological conditions
43 *FBP2* forms dimers and tetramers, thus we speculate that WT-*FBP2* and V115M-*FBP2* co-
44
45
46
47
48
49
50
51
52
53
54
55
56
57
58
59
60

1
2
3 expressed in a cell form heteromers with reduced enzyme activity and stability explaining a
4 dominant negative effect of the variant. The role of gluconeogenesis in the brain, where FBP2
5 but not FBP1 is expressed, is not fully understood but there is evidence that it is an important
6 part of the local energy metabolism under physiological and pathological conditions (Yip *et al.*,
7 2016). In fructose-1,6-bisphosphate deficiency of the liver enzyme FBP1, acute attacks with
8 hypoglycemia and lactic acidosis are often triggered by febrile infections. In the 3 index patients
9 described here, the severe crisis also followed a febrile infection and lactate was elevated in the
10 white matter during the acute phase on MRS. These findings indicate that defective
11 gluconeogenesis might contribute to the pathophysiology. As synthesis of myelin is a very
12 energy consuming process the oligodendrocytes might be particularly vulnerable to such a
13 defect during the phase of intense myelination at the at the end of the first year of life (Harris
14 and Attwell, 2012).

15
16
17 On fibroblast analysis, WT-FBP2 was increased in the fibroblasts of patient III.5. Presumably,
18 this was due to reduced FBP2 function in the cell, and subsequent upregulation of FBP2
19 expression. We were also able to demonstrate preferential clearing of the defective protein by
20 ERLAD leading to upregulation of LAMP-1 expression. These findings further support
21 pathogenicity of the variant.

22
23
24 As recently reviewed by Huangyang *et al.*, insights from cancer research have shown that many
25 metabolic enzymes have activities outside of their established metabolic roles, including the
26 regulation of gene expression, DNA damage repair, cell cycle progression and apoptosis
27 (Huangyang and Simon, 2018). The authors speculate that modulating gene expression by
28 metabolic enzymes facilitates adaptation of the cell to rapidly changing environments. A
29 recently described example of a genetic defect that only affects the non-canonical functions of
30 a metabolic enzyme involves the HK1 gene. Autosomal recessive mutations in the HK1 gene,
31 coding for hexokinase 1, lead to a loss of enzymatic function and cause non-spherocytic
32 hemolytic anemia. However, heterozygous de novo missense mutations in the same gene
33 detected recently in six patients with developmental delay, intellectual disability, structural
34 brain abnormality, and visual impairment, were associated with normal hexokinase activity
35 (Okur *et al.*, 2019).

36
37
38 FBP2 reportedly also has several other functions in addition to enzymatic activity. Firstly, an
39 involvement in mitochondrial protection has been shown. Upon activation of glycolysis by
40 insulin, FBP2 colocalizes with mitochondria resulting in a reduced rate of calcium-induced
41 mitochondrial swelling and protection of ATP synthesis (Gizak *et al.*, 2012). We analyzed the
42
43
44
45
46
47
48
49
50
51
52
53
54
55
56
57
58
59
60

1
2
3 effect of the V115M-FBP2 variant on mitochondria in fibroblasts of patient III.5 and found a
4 pronounced disturbance of the mitochondrial network. In fact, the V115M-FBP2 variant did
5 not colocalize with mitochondria, and ROS production in the organelles and whole cell was
6 increased. Also supportive of mitochondrial dysfunction was evidence of elevated lactate levels
7 in the white matter during the acute attack and subsequent normalization over the following
8 months coinciding with clinical improvement. Interestingly, the MRI pattern seen in our
9 patients matches that seen in Kearns-Sayre or Leigh syndrome, both classical mitochondrial
10 disorders (van der Knaap, 2005). However, such patients have a progressive disease course
11 with grey matter pathology especially of the basal ganglia which was not seen in the patients
12 described here. In conclusion, while we collectively have evidence suggesting the
13 pathophysiology of the disorder described in this article involves mitochondrial dysfunction, it
14 does not, however, resemble a classical mitochondrial disorder.

15
16 A further function attributed to FBP2 is regulation of nuclear processes. Like many glucose
17 metabolism enzymes, FBP2 has a classical Nuclear Localization Sequence (Gizak *et al.*, 2009).
18 FBP2 interacts with histone and non-histone nuclear proteins and has been found to restrain
19 mitochondrial biogenesis and respiration by colocalization with the c-Myc transcriptions factor
20 (Mamczur *et al.*, 2012; Huangyang *et al.*, 2020). Furthermore, in cardiomyocytes and cancer
21 cells, FBP2 has a recognized role in the regulation of the cell cycle (Gizak *et al.*, 2006).
22 Immunostaining patient III.5 fibroblasts we were not able to detect FBP2 in nuclei. This
23 suggests a dominant negative effect of V115M-FBP2 on nuclear localization, presumably due
24 to heteromerization of WT and mutant proteins, and indicates that the nuclear functions of FBP2
25 are diminished in *FBP2* related-leukodystrophy.

26
27 We conducted a search using the GeneMatcher database for further families with a similar
28 phenotype and variants in the *FBP2* gene and inquired with other international specialists in
29 leukodystrophies if they had seen similar cases but were so far unsuccessful (Sobreira *et al.*,
30 2015). It is possible that only variants that affect both the enzymatic function and the non-
31 canonical functions of FBP2 will be associated with the clinical phenotype seen in the family
32 described here. Furthermore, FBP2-related leukodystrophy is, no doubt, an extremely rare
33 disorder and misinterpretation as an autoinflammatory disorder such as acute disseminated
34 encephalomyelitis, the initial diagnosis in patients III.2 and III.5, may hamper recognition of
35 further cases.

36
37 In conclusion, we report on a novel disorder that we termed *FBP2*-related leukodystrophy. The
38 phenotype is characterized by a metabolic crisis at the end of the first year of life leading to
39 widespread demyelination and loss of abilities. The patients recover over several months

1
2
3 regaining normal development accompanied by remyelination. The variant in *FBP2* that was
4 found to segregate in the family with the disorder, damages not only the enzymatic activity but
5 also the non-canonical functions of *FBP2* involved in mitochondrial protection and nuclear
6 localization. *FBP2*-related leukodystrophy is a novel member of the group of remitting
7 leukodystrophies.
8
9
10
11
12
13
14

15 **Funding:** This work was supported by the German Research Foundation (DFG, Ga354/14-1,
16 HU 941/2-5), die Niedersächsisches Ministerium für Wissenschaft und Kultur (11-76251-12-
17 4/12 (ZN2938)) and by the Polish National Science Centre (UMO-2015/19/B/NZ1/00332)
18
19
20
21
22

23 **Competing interest:** The authors report no competing interests.
24
25
26
27
28
29
30
31
32
33
34
35
36
37
38
39
40
41
42
43
44
45
46
47
48
49
50
51
52
53
54
55
56
57
58
59
60

References

- Al-Robaiy S, Eschrich K. Rat muscle fructose-1,6-bisphosphatase: cloning of the cDNA, expression of the recombinant enzyme, and expression analysis in different tissues. *Biol Chem* 1999; 380(9): 1079-85.
- Barciszewski J, Wisniewski J, Kolodziejczyk R, Jaskolski M, Rakus D, Dzugaj A. T-to-R switch of muscle fructose-1,6-bisphosphatase involves fundamental changes of secondary and quaternary structure. *Acta Crystallogr D Struct Biol* 2016; 72(Pt 4): 536-50.
- Dewulf JP, Wiame E, Dorboz I, Elmaleh-Berges M, Imbard A, Dumitriu D, *et al.* SLC13A3 variants cause acute reversible leukoencephalopathy and alpha-ketoglutarate accumulation. *Ann Neurol* 2019; 85(3): 385-95.
- Dreha-Kulaczewski SF, Brockmann K, Henneke M, Dechent P, Wilken B, Gartner J, *et al.* Assessment of myelination in hypomyelinating disorders by quantitative MRI. *J Magn Reson Imaging* 2012; 36(6): 1329-38.
- Duda P, Janczara J, McCubrey JA, Gizak A, Rakus D. The Reverse Warburg Effect is Associated with Fbp2-Dependent Hif1alpha Regulation in Cancer Cells Stimulated by Fibroblasts. *Cells* 2020; 9(1).
- Frahm J, Bruhn H, Gyngell ML, Merboldt KD, Hanicke W, Sauter R. Localized high-resolution proton NMR spectroscopy using stimulated echoes: initial applications to human brain in vivo. *Magn Reson Med* 1989; 9(1): 79-93.
- Fregno I, Fasana E, Bergmann TJ, Raimondi A, Loi M, Solda T, *et al.* ER-to-lysosome-associated degradation of proteasome-resistant ATZ polymers occurs via receptor-mediated vesicular transport. *EMBO J* 2018; 37(17).
- Gizak A, Dzugaj A. FBPase is in the nuclei of cardiomyocytes. *FEBS Lett* 2003; 539(1-3): 51-5.
- Gizak A, Maciaszczyk-Dziubinska E, Jurowicz M, Rakus D. Muscle FBPase is targeted to nucleus by its 203KKKGK207 sequence. *Proteins* 2009; 77(2): 262-7.
- Gizak A, McCubrey JA, Rakus D. Cell-to-cell lactate shuttle operates in heart and is important in age-related heart failure. *Aging (Albany NY)* 2020; 12(4): 3388-406.
- Gizak A, Pirog M, Rakus D. Muscle FBPase binds to cardiomyocyte mitochondria under glycogen synthase kinase-3 inhibition or elevation of cellular Ca²⁺ level. *FEBS Lett* 2012; 586(1): 13-9.
- Gizak A, Wrobel E, Moraczewski J, Dzugaj A. Changes in subcellular localization of fructose 1,6-bisphosphatase during differentiation of isolated muscle satellite cells. *FEBS Lett* 2006; 580(17): 4042-6.
- Gurgel-Giannetti J, Lynch DS, Paiva ARB, Lucato LT, Yamamoto G, Thomsen C, *et al.* A novel complex neurological phenotype due to a homozygous mutation in FDX2. *Brain* 2018; 141(8): 2289-98.
- Harris JJ, Attwell D. The energetics of CNS white matter. *J Neurosci* 2012; 32(1): 356-71.
- Helms G, Dathe H, Dechent P. Quantitative FLASH MRI at 3T using a rational approximation of the Ernst equation. *Magn Reson Med* 2008a; 59(3): 667-72.
- Helms G, Dathe H, Dechent P. Modeling the influence of TR and excitation flip angle on the magnetization transfer ratio (MTR) in human brain obtained from 3D spoiled gradient echo MRI. *Magn Reson Med* 2010; 64(1): 177-85.
- Helms G, Dathe H, Kallenberg K, Dechent P. High-resolution maps of magnetization transfer with inherent correction for RF inhomogeneity and T1 relaxation obtained from 3D FLASH MRI. *Magn Reson Med* 2008b; 60(6): 1396-407.
- Houck SA, Ren HY, Madden VJ, Bonner JN, Conlin MP, Janovick JA, *et al.* Quality control autophagy degrades soluble ERAD-resistant conformers of the misfolded membrane protein GnRHR. *Mol Cell* 2014; 54(1): 166-79.
- Huangyang P, Li F, Lee P, Nissim I, Weljie AM, Mancuso A, *et al.* Fructose-1,6-Bisphosphatase 2 Inhibits Sarcoma Progression by Restraining Mitochondrial Biogenesis. *Cell Metab* 2020; 31(1): 174-88 e7.
- Huangyang P, Simon MC. Hidden features: exploring the non-canonical functions of metabolic enzymes. *Dis Model Mech* 2018; 11(8).
- Li H, Handsaker B, Wysoker A, Fennell T, Ruan J, Homer N, *et al.* The Sequence Alignment/Map format and SAMtools. *Bioinformatics* 2009; 25(16): 2078-9.

- 1
2
3 Lopez-Hernandez T, Ridder MC, Montolio M, Capdevila-Nortes X, Polder E, Sirisi S, *et al.* Mutant
4 GlialCAM causes megalencephalic leukoencephalopathy with subcortical cysts, benign familial
5 macrocephaly, and macrocephaly with retardation and autism. *Am J Hum Genet* 2011; 88(4): 422-32.
6 Mamczur P, Borsuk B, Paszko J, Sas Z, Mozrzyms J, Wisniewski JR, *et al.* Astrocyte-neuron crosstalk
7 regulates the expression and subcellular localization of carbohydrate metabolism enzymes. *Glia* 2015;
8 63(2): 328-40.
9 Mamczur P, Sok AJ, Rzechonek A, Rakus D. Cell cycle-dependent expression and subcellular localization
10 of fructose 1,6-bisphosphatase. *Histochem Cell Biol* 2012; 137(1): 121-36.
11 McKenna A, Hanna M, Banks E, Sivachenko A, Cibulskis K, Kernytsky A, *et al.* The Genome Analysis
12 Toolkit: a MapReduce framework for analyzing next-generation DNA sequencing data. *Genome Res*
13 2010; 20(9): 1297-303.
14 Okur V, Cho MT, van Wijk R, van Oirschot B, Picker J, Coury SA, *et al.* De novo variants in HK1 associated
15 with neurodevelopmental abnormalities and visual impairment. *Eur J Hum Genet* 2019; 27(7): 1081-9.
16 Pouwels PJ, Brockmann K, Kruse B, Wilken B, Wick M, Hanefeld F, *et al.* Regional age dependence of
17 human brain metabolites from infancy to adulthood as detected by quantitative localized proton MRS.
18 *Pediatr Res* 1999; 46(4): 474-85.
19 Provencher SW. Estimation of metabolite concentrations from localized in vivo proton NMR spectra.
20 *Magn Reson Med* 1993; 30(6): 672-9.
21 Rimmer A, Phan H, Mathieson I, Iqbal Z, Twigg SRF, Consortium WGS, *et al.* Integrating mapping-,
22 assembly- and haplotype-based approaches for calling variants in clinical sequencing applications. *Nat*
23 *Genet* 2014; 46(8): 912-8.
24 Schneider CA, Rasband WS, Eliceiri KW. NIH Image to ImageJ: 25 years of image analysis. *Nat Methods*
25 2012; 9(7): 671-5.
26 Sobreira N, Schietecatte F, Valle D, Hamosh A. GeneMatcher: a matching tool for connecting
27 investigators with an interest in the same gene. *Hum Mutat* 2015; 36(10): 928-30.
28 van der Knaap MS, Bugiani M. Leukodystrophies: a proposed classification system based on
29 pathological changes and pathogenetic mechanisms. *Acta Neuropathol* 2017; 134(3): 351-82.
30 van der Knaap MSV, J. Magnetic Resonance of Myelination and Myelin Disorders. 3rd ed. Berlin
31 Heidelberg; 2005.
32 Wisniewski J, Pirog M, Holubowicz R, Dobryszyci P, McCubrey JA, Rakus D, *et al.* Dimeric and
33 tetrameric forms of muscle fructose-1,6-bisphosphatase play different roles in the cell. *Oncotarget*
34 2017; 8(70): 115420-33.
35 Yan H, Helman G, Murthy SE, Ji H, Crawford J, Kubisiak T, *et al.* Heterozygous Variants in the
36 Mechanosensitive Ion Channel TMEM63A Result in Transient Hypomyelination during Infancy. *Am J*
37 *Hum Genet* 2019; 105(5): 996-1004.
38 Yip J, Geng X, Shen J, Ding Y. Cerebral Gluconeogenesis and Diseases. *Front Pharmacol* 2016; 7: 521.
39 Zarzycki M, Kolodziejczyk R, Maciaszczyk-Dziubinska E, Wysocki R, Jaskolski M, Dzugaj A. Structure of
40 E69Q mutant of human muscle fructose-1,6-bisphosphatase. *Acta Crystallogr D Biol Crystallogr* 2011;
41 67(Pt 12): 1028-34.
42
43
44
45
46
47
48
49
50
51
52
53
54
55
56
57
58
59
60

Figure legends

Figure 1: Pedigree and segregation analysis of the affected Family. Nomenclature is according to GenBank accession number NM_003837.2. Case reports on III.2, III.5 and IV.1 can be found in the results section. I.2, female, was born in 1948 and developed epilepsy and schizophrenia during her youth. She has never learnt a profession and lives in a shelter home. Her two children, II.2 II.4, grew up in an orphanage in the GDR because she was incapable of looking after her. No information is available for the first 5 years of their life. Patient II2 developed severe anorexia as a teenager, which currently at age 47 is still present and prevents her from working in her profession as a nurse. II.4, developed epilepsy at age 4 years, and still now requires anticonvulsive medication at age 46. She works as a cleaner. III.3, aged 26 years, has a history of psychosis and drug addiction. He refused cerebral MRI investigation. III.4 developed epilepsy at age 9 years following a presumed viral infection with high fever. Development up to this point of time was normal with no signs of a metabolic crisis. She was treated with oxcarbazepine but continued to have two brief (2-3 minutes) focal seizures a month until age 13 years. At last presentation at age 14.5 years she was seizure free and visiting a regular school. IV.2, now aged 6 years, has mildly delayed speech development and an attention deficit hyperactivity disorder. Family members I.1, II.1, II.3, II5 and III.1 have no known neurological or psychiatric disorders.

Figure 2: MR imaging of the family members. A-K) Axial MR images of the patients with the remitting leukodystrophy. A-C) T2 weighted images of patient III.2 at age 14 months, 22 months and 20 years. D-G) T2 weighted images of patient III.5 at age 11 months, 21 months, 32 months and 24 years. H-K) T2 weighted images of patient IV.1 at age 13, 19, 25 and 29 months. L-O) ADC of patient IV.1 at corresponding time points. P, Q) T2 weighted images of patient III.4 at age 10 (P) and 15 years (Q) with residual WM lesions, pronounced frontally and in the genu corpus callosum. R) FLAIR images of patient II.2 at age 38 years revealing frontally pronounced residual WM lesion. S) FLAIR images of patient II.4 at age 46 years with similar residual pattern and global atrophy. T) T2 weighted images of patient IV.2 at age 4 years. Of note are the subtle WM hyperintensities in genu and splenium, comparable to patient III.4, II.2, II.4, although no metabolic crisis occurred.

Figure 3: Quantitative MR spectroscopy and Myelin sensitive imaging. A) Lactate levels (in mM) in patients III.2, III.5 and IV.1 at different time points. Over time lactate returned to normal ranges (≤ 1 mM) in the two follow up studies. B – D) Overlay of color-coded axial MTsat maps onto corresponding T1 weighted images of patient IV.1. At age 13 months (B)

1
2
3 blue color-coded white matter areas depict myelin deficit; at 19 months (C) extension of blue-
4 gray color-coded WM regions and appearance of light blue-coded WM frontally representing
5 very low MT values (close to CSF) reveal ongoing demyelination; at 29 months (D) appearance
6 of gray-red-orange-yellow color-coded WM areas illustrate remyelination. E) Overlay of color-
7 coded axial MTsat map onto corresponding T1 weighted image of a healthy control age 18m
8 and the color scale encoding the MTsat values. Note the predominance of red-orange coded
9 MTsat values and transition to yellow coded WM pointing to sufficient myelination.
10
11
12
13
14
15

16 **Figure 4: Comparison of kinetics and stability of the FBP2 variants.**

17 A) Comparison of V115M-FBP2 and WT-FBP2 kinetic parameters, and B) thermal stability of
18 the mutant protein. In the panel B), solid lines represent mean melting curves from three
19 independent measurements, and dashed lines indicate mean melting temperatures. C)
20 Enzymatic activity of V115M-FBP2 and WT-FBP2 after prolonged incubation at 37°C. The
21 activity was normalized to mean activity at t=0 for the respective FBP2 form.
22
23
24
25
26
27

28 **Figure 5: Subcellular localization of the FBP2 variants.**

29 A) In healthy control fibroblasts (HCF), FBP2 is homogeneously distributed in whole
30 cytoplasm and nuclei (arrows), as determined by immunocytochemistry. In fibroblasts derived
31 from patient III.5 (Leucodystrophy Fibroblasts, LeuF), nuclei (arrows) are empty, and the
32 enzyme accumulates only in their vicinity, not in cellular protrusions. B) GSK3 β inhibition
33 results in accumulation of FBP2-related immunofluorescent signal with mitochondria in HCF,
34 but not in LeuF. C) In control conditions, FITC-labeled V115M-FBP2 does not co-localize with
35 mitochondria of HCF, while WT-FBP2 does (arrows). D) Mitochondrial network in LeuF is
36 much less developed and membrane of the organelles is less polarized than in HCF. Total as
37 well as mitochondrial production of reactive oxygen species (ROS) in LeuF is higher than in
38 HCF.
39
40
41
42
43
44
45
46
47
48

49 **Figure 6: Expression and degradation of the FBP2 variants.**

50 A) Total fluorescent signal associated with polyclonal antibodies against FBP is stronger in
51 Leucodystrophy Fibroblasts (LeuF) than in healthy control fibroblasts (HCF). B) Similarly, the
52 signal for total FBP2 mRNA is much stronger in LeuF than in HCF. V115M-FBP2 mRNA is
53 not detected in HCF. C) In HCF, FITC-labeled WT-FBP2 hardly co-localizes with ER while
54 V115M-FBP2 highly co-localizes with ER in control conditions, but not after ERAD inhibition.
55 D) Total fluorescent signal associated with K48 polyubiquitination is slightly but significantly
56
57
58
59
60

1
2
3 stronger in LeuF than in HCF. E) The majority of FBP-related granules co-localize with
4 proteasome subunit PSMC6. F) LAMP-1 level is over 2.5-times higher in LeuF than in HCF.
5
6
7
8

9 **Supplementary Figure 1: Confirmation of heterozygous *FBP2* variant.** A) Sanger
10 sequencing chromatogram of the *FBP2* mutation side is shown for each investigated family
11 member with different mutation status wild type (WT) and heterozygous mutated (het). The
12 position of the affected *FBP2* nucleotide triplet coding for p.V115M is highlighted by a box.
13 Nomenclature is according to GenBank accession number NM_003837.2 and NP_003828.2.
14
15
16
17
18
19
20

21 **Supplementary Figure 2: Multiple Alignment and stereo representation of Val115**
22 **position in the FBP2 structure.** A) The multiple alignment shows that the Val115 position is
23 strongly conserved with hydrophobic residues for FBP in vertebrates, but also insects, plant,
24 whereas there is an Ala as an even smaller hydrophobic side chain with *Aspargillus*. B) Stereo
25 view „crossed eye“ of FBP2 subunit A with structural elements in schematic representation.
26 Val115 space filling in red, surrounding hydrophobic residues Val94, Tyr140, Ala153, and the
27 carbon backbone of Lys142 side chain in green, subunit C in dark blue. The figure was drawn
28 with WebLab-Viewer (Molecular Simulations Inc., Burlington, MA, USA), using the X-ray
29 structure of human FBP2 (pdb code 5et7).
30
31
32
33
34
35
36
37
38
39

40 **Supplementary Table 1: Basic WES information and output data.** Overview of coverage,
41 mapping information and homozygosity for each WES sample. Consanguinity can be estimated
42 using % of rare hom variants (3 – 6%) and autosomal runs of homozygosity (> 200 – 300 mb).
43 Cov, coverage; hom, homozygosity
44
45
46
47
48
49

50 **Supplementary Table 2: Detected filtered common variants.** Detailed variant information
51 with localization, substitution and occurrence within the family. Het, heterozygous
52
53
54

55 **Supplementary Table 3: Detected filtered common variants.** Detailed variant information
56 corresponding bioinformatic prediction on the functional effect, conservation and occurrence
57 in ExAC. Variant classification for each tool was obtained using dbNSFP version 3.4.
58
59
60

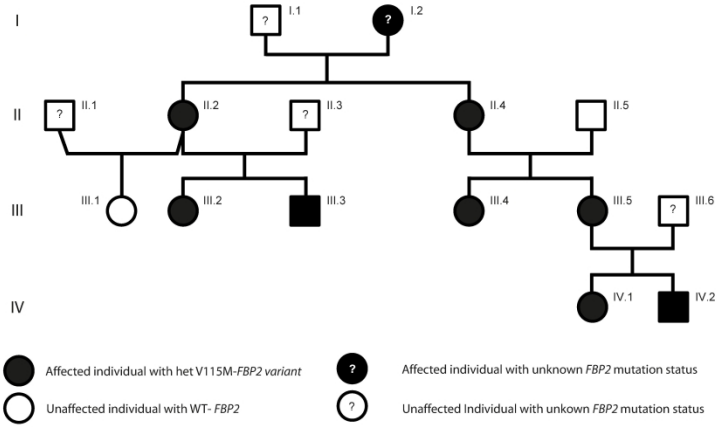


Figure 1

Figure 1

210x297mm (600 x 600 DPI)

1
2
3
4
5
6
7
8
9
10
11
12
13
14
15
16
17
18
19
20
21
22
23
24
25
26
27
28
29
30
31
32
33
34
35
36
37
38
39
40
41
42
43
44
45
46
47
48
49
50
51
52
53
54
55
56
57
58
59
60

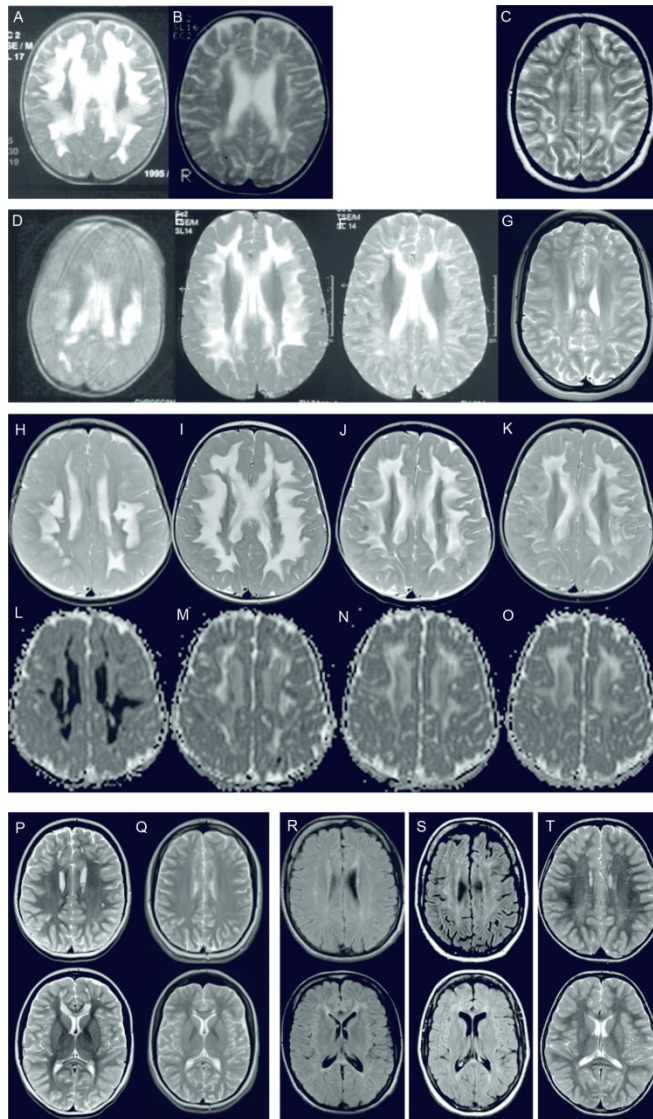


Figure 2

Figure 2

135x248mm (300 x 300 DPI)

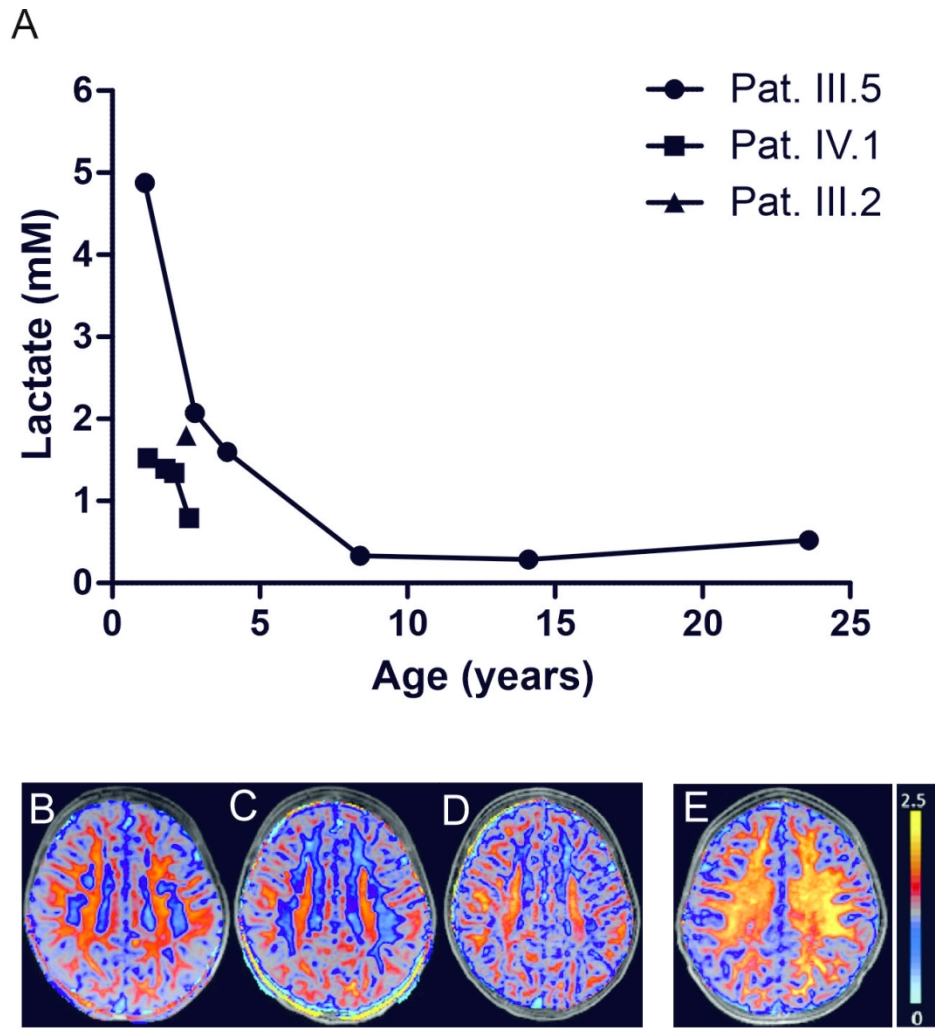


Figure 3

Figure 3

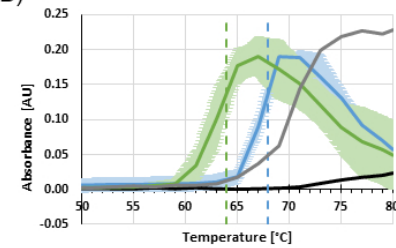
111x141mm (300 x 300 DPI)

A)

FBP2	k_{cat} [s^{-1}]	K_s [μM]	K_{si} [μM]	n , F-1,6-BP	IC_{50} AMP [μM]	n , AMP
WT	20.96 ± 2.52	3.66 ± 0.08	111 ± 2	1.61 ± 0.036	0.592 ± 0.01	2.04 ± 0.0515
V115M	11.47 ± 0.22	5.39 ± 0.19	167.7 ± 8.55	1.32 ± 0.03	1.23 ± 0.14	1.187 ± 0.099

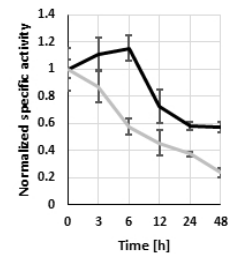
Data are presented as mean \pm SD k_{cat} – catalytic constant, K_s – substrate constant, K_{si} – substrate inhibition constant, n – Hill coefficient, IC_{50} – half inhibition constant

B)



— Melting curve for V115M FBP2 R-state
- - - Mean melting temperature for V115M FBP2 R-state
— Melting curve for V115M FBP2 T-state
- - - Mean melting temperature for V115M FBP2 T-state
— Melting curve for WT FBP2 R-state
— Melting curve for WT FBP2 T-state

C)



— WT FBP2
— V115M FBP2

Figure 4

Figure 4

190x275mm (96 x 96 DPI)

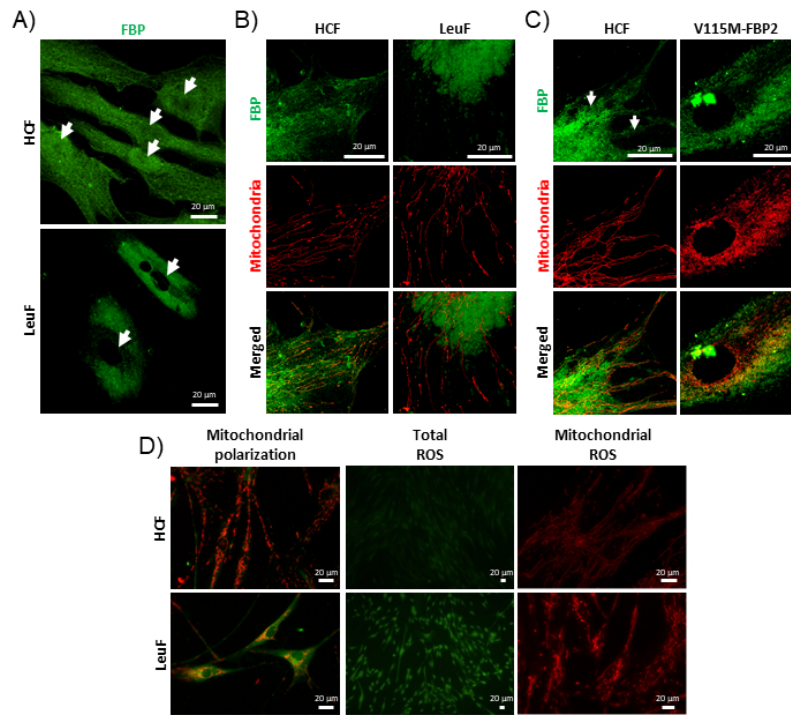


Figure 5

Figure 5

190x275mm (96 x 96 DPI)

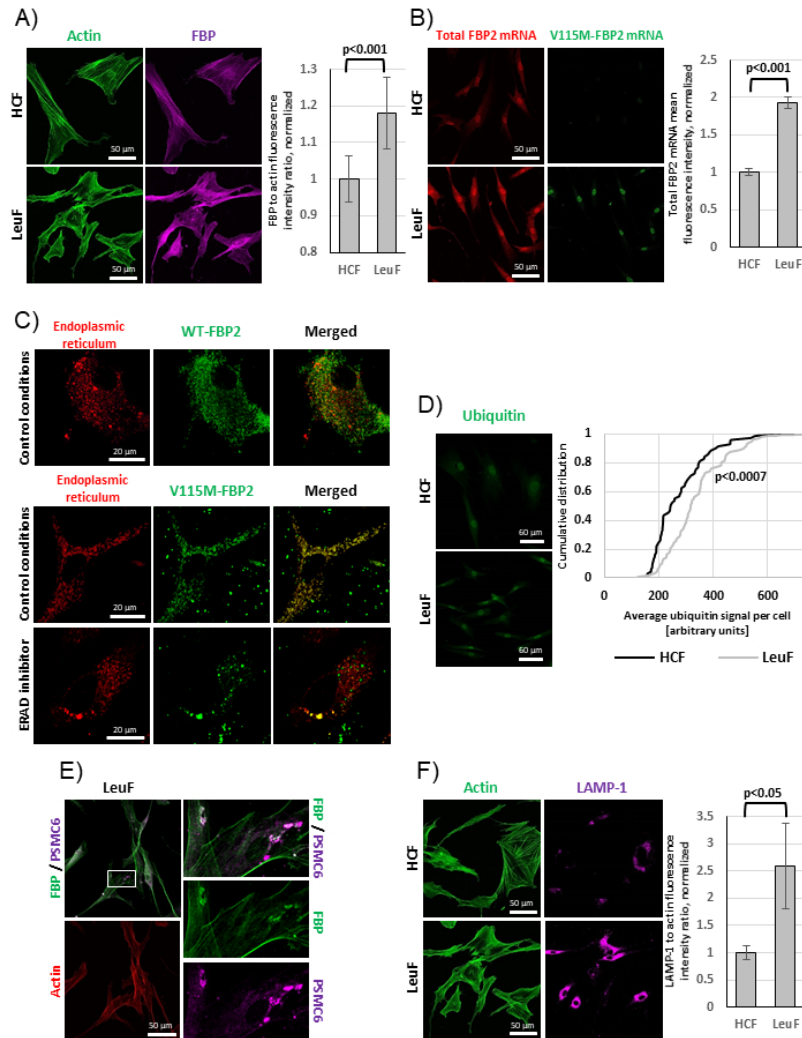
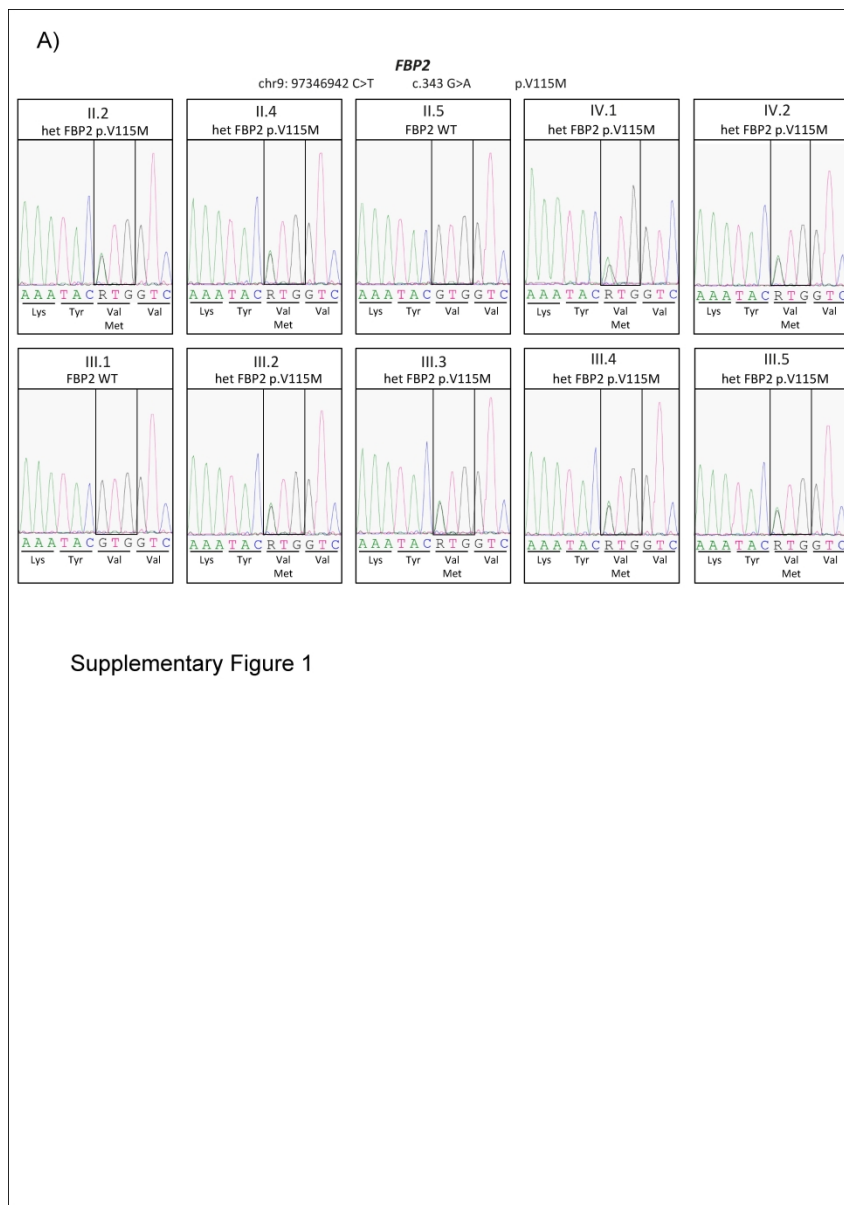


Figure 6

Figure 6

190x275mm (96 x 96 DPI)



210x297mm (600 x 600 DPI)

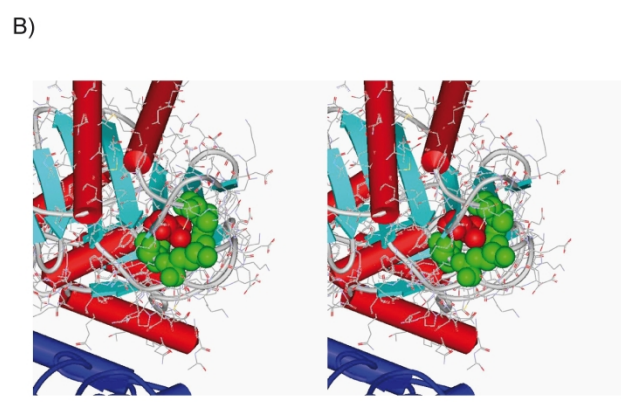
A)

```

130      140      150      160      170      180
|        |        |        |        |
F16P2_HUMAN IAGSVNVTGDEVKRLDVLNSLIVNMVQSSYSTCYLVSEENKDAIITAKEKRGKRYVCFD
Bos_taurus IAGSVNVTGDEVKRLDVLNSLIVNMVQSSYSTCYLVSEENKDAIITAKEKRGKRYVCFD
Gallus_gallus_FBP2 IAGTVNVTGDEVKRLDVLNSLIVNMVQSSYSTCYLVSEENKDAIITAKEKRGKRYVCFD
Xenopus_tropicalis ISGTVNVTGDEVKRLDVLNSLIVNMVQSSYSTCYLVSEENKDAIITAKEKRGKRYVCFD
Danio_rerio IAGQVNVVTGDEVKRLDVLNSLIVNMVQSSYSTCYLVSEENKDAIITAKEKRGKRYVCFD
human_FBP1 IAGSTVNVTDQVKKLDVLSNDLVMNMLKSSFATCVLVSEEDKRAIIVEPEKRGKRYVCFD
Anopheles_Gambiae_FBP ISGDTNVQGEQVKKLDVLSNEIFINMLKSSYATCLVSEENNVVIEIETDKRGKRYVCFD
Glycine_max_FBP1 VQGANVNVQGEQVKKLDVLSNEIVSNCLRSSGRTGIIASSEEDNPAVEESVSNYIVVFD
Aspargillus_niger_FBP LAGSSNTGDDQKLDVIGNDIFISAMKSGKCRILVSEEEEAIVFDEHFNARYAVVCD
Prim.cons. IAGSVNVTGDEVKRLDVLNSLIVNML2SSYSTCYLVSEENKDAIITAKEKRGKRYVCFD

190      200      210      220      230      240
|        |        |        |        |
F16P2_HUMAN PLDGSSNIDCLASIGTIFAIYRKTSE-----DEPSEKDALQCGRNIVAAGY
Bos_taurus PLDGSSNIDCLASIGTIFAIYRKTSE-----DEPSEKDALQCGRNIVAAGY
Gallus_gallus_FBP2 PLDGSSNIDCLAPIGTIFAIYKRETD-----DEPSEKDALQCGRNIVAAGY
Xenopus_tropicalis PLDGSSNIDCLASIGTIFAIYRRTD-----TEPSEQDALQCGRNIVAAGY
Danio_rerio PLDGSSNIDCLAPIGTIFAIYKRISD-----GEFSEKDALQCGNQIVCAGY
human_FBP1 PLDGSSNIDCLVSVGTIFGIYRKRST-----DEPSEKDALQCGRNIVAAGY
Anopheles_Gambiae_FBP PLDGSSNIDCLVSGISIFAITKQVKEN-----TTFSEKDALQCGRNIVAAGY
Glycine_max_FBP1 PLDGSSNIDAAVSTGSIFGIYFNDECLADIDDDPTLDTEQRCIVNVQCGSNLLAAGY
Aspargillus_niger_FBP PLDGSSNLDAGVSVGTIFEIFKLPDEVLGN-----NKVTAQLLRACETKVASGF
Prim.cons. PLDGSSNIDCLASIGTIFAIY2KTSE3L222DDPTLDITTEPSEKDALQCGRNIVAAGY

```



Supplementary figure 2

210x297mm (600 x 600 DPI)

Sample	Varbank Pipeline	read length	Mean Cov	Cov 30x	Total reads	Unique mapped reads [%]	autosomal Runs of Homozygosity [Mb]	% of rare hom variants	Gender
II.2	v 3.5	101	95	86.0	122789264	79.00	15	0.1	Female
II.4	v 3.5	101	83	83.1	107980136	78.85	21	0.4	Female
III.2	v 3.4	76	75	81.9	132206850	74.67	8	0.1	Female
III.4	v 3.4	76	66	72.9	115661122	74.87	7	0.1	Female
III.5	v 3.5	101	74	76.9	100459852	82.61	34	0.0	Female
IV.1	v 3.5	101	73	80.7	106791788	87.73	14	0.0	Female

Supplementary Table 1

1
2
3
4
5
6
7
8
9
10
11
12
13
14
15
16
17
18
19
20
21
22
23
24
25
26
27
28
29
30
31
32
33
34
35
36
37
38
39
40
41
42
43
44
45
46
47
48
49
50
51
52
53
54
55
56
57
58
59
60

Gene	Chr	Position	Ref	Mut	Transcript ID	cDNA	Protein	Sample					
								II.2	II.4	III.2	III.4	III.5	IV.1
<i>CCT6</i> A	7	56055733	T	C	NM_001762.3	c.446T>C	p.Ile149Thr	he t	he t	he t	he t	he t	he t
<i>FBP2</i>	9	94584660	C	T	NM_003837. 3	c.343G>A	p.Val115Me t	he t	he t	he t	he t	he t	he t

Supplementary Table 2

For Review Only

			CCT6A		FBP2	
			NM_001762.3		NM_003837.3	
			p.I149T	Prediction	p.V115M	Prediction
			Tool	Range		
			Median Rank Score	0 - 1	0.48	0.65
FUNCTIONAL PREDICTION SCORES	SIFT	0 - 1	0.176	Tolerated	0.011	Damaging
	PolyPhen2	0 - 1	0.009	Benign	0.999	Damaging
	LRT	0 - 1	0.000290	Neutral	0.000	Damaging
	MutTaster	0 - 1	0.998	Damaging	1.000	Damaging
	MutAssessor	-5.545 - 5.975	1.3	Low functional impact	2.535	Medium functional impact
	FATHMM	-16.13 - 10.64	-1.15	Tolerated	-0.74	Tolerated
	PROVEAN	-14 - 14	-2.39	Neutral	-2.26	Neutral
	VEST3	0 - 1	0.195	Tolerated	0.638	Damaging
	MetaSVM	-2 - 3	-0.7441	Tolerated	0.1394	Damaging
	MetaLR	0 - 1	0.2964	Tolerated	0.5455	Damaging
	CADD	-7.5350 - 35.7885	1.3315	Neutral	5.6513	Damaging
	DANN	0 - 1	0.8208	Neutral	0.9987	Damaging
	FitCons	0 - 1	0.7354	Functional important	0.5731	Less Functional important
CONSERVATION SCORES	GERP	-12.3 - 6.17	2.39	High conserved	4.08	High conserved
	PhastCons	0 - 1	0.996	High conserved	0.980	High conserved
	PHYLOP20	-13.282 to 1.199	0.824	High conserved	0.876	High conserved

Supplementary Table 3